PERIÓDICO TCHÊ QUÍMICA
ARTIGO ORIGINAL

MÉTODOS ESPECTROSCÓPICOS PARA A DETERMINAÇÃO DE GEOTITA EM CAULINITA

SPECTROSCOPIC METHODS TO DETERMINATION OF GEOTHITE IN KAOLINITE

DE SOUZA, Marcelo Kehl[1]; KLUNK, Marcos Antônio[2]*; XAVIER, Soyane Juceli Siqueira[1]; DAS, Mohuli[3]; DASGUPTA, Sudipta[3]

[1] Department of Geology, University of Vale do Rio dos Sinos, Av. Unisinos 950, São Leopoldo, RS, Brazil

[2] Department of Mechanical Engineering, University of Vale do Rio dos Sinos, São Leopoldo, RS, Brazil

[3] Department of Earth Sciences, Indian Institute of Technology Bombay (IIT Bombay), Powai, India

** Autor correspondente*
e-mail: marcosak@edu.unisinos.br

Received 01 April 2020; received in revised form 27 May 2020; accepted 29 May 2020

RESUMO

Um dos principais contaminante da caulinita, o ferro, impacta diretamente na qualidade em seu valor comercial. O monitoramento espectroscópico, medido a profundidade da absorção da caulinita, é comparado com a literarura a fim de identificar possíveis contaminantes. A ocorrência da caulinita se deve à formação a de minerais primários após a liberação parcial de cátions e sílicio. Este argilo-mineral tem uma forma simples, com imperfeições cristalográficas variáveis, especialmente na presença de ferro, que substituem o alumínio na cadeia mineral, causando várias desorganizações estruturais. A extração de minerais industriais combinada com estudos geológicos, permite o desenvolvimento de novas fontes de energia, como minerais argilosos, em particular caulinita. Dependendo da origem das caulinitas, apresença de óxidos de ferro em sua estrutura, Fe_2O_3 e FeO(OH) são comuns. Ao comparar os resultados da espcetroscopia (fluorescenica de raio-X, difração de raio-x; RAMAN) e no imagiamento através do MEV-EDS, foi possível identificar a caulinita, com maior coeficiente de determinação, quando a proporção de caulinita atinge 60% ou mais na mistura. A caulinita pode ser identificada e quantificada com alta correlação na mistura a partir da absorção da amostra. Assim, o método possui grande potencial para auxiliar na quantificação e, consequentemente, na discriminação da qualidade da caulinita.

Palavras-chave: *Goetita, Argilo-minerais; Espectroscopia.*

ABSTRACT

One of the main contaminants of kaolinite, the iron, directly impacts quality in its commercial value. The spectroscopic monitoring, measured the depth of absorption of kaolinite, is compared with the literature in order to identify possible contaminants. The occurrence of kaolinite is due to the formation of primary minerals after the partial release of cations and silicon. This clay-mineral has a simple shape, with variable crystallographic imperfections, especially in the presence of iron, which replaces aluminum in the mineral chain, causing various structural disorganizations. The extraction of industrial minerals combined with geological studies, allows the development of new sources of energy, such as clay minerals, in particular kaolinite. Depending on the origin of the kaolinites, the presence of iron oxides in its structure, Fe_2O_3 and FeO(OH), are common. By comparing the results of spectroscopy (X-ray fluorescence, X-ray diffraction, RAMAN) and imaging using SEM-EDS, it was possible to identify kaolinite, with a higher determination coefficient, when the proportion of kaolinite reaches 60% or more in the mix. Kaolinite can be identified and quantified with a high correlation in the mixture from the sample absorption. Thus, the method has great potential to assist in quantifying and, consequently, in discriminating the quality of kaolinite.

Keywords: *Goethite; Clay Minerals; Spectroscopy.*

DOI: 10.52571/PTQ.v17.n35.2020.27_KLUNK_pgs_303_314.pdf

1. INTRODUCTION

Brazil's extractive economy is mainly focused on supplying the metalworking industry (Schrecker *et al.,* 2018; Giacomin *et al.,* 2017; Paulino, 2014). About 85% by volume are of metallic minerals extracted in the country, and the other 15% are non-metallic (Macedo *et al.,* 2003; De Souza *et al.,* 2019). The extraction of industrial minerals combined with geological studies allows the development of new energy sources such as clay-minerals, in particular, kaolinite (Sruthi and Reddy, 2017). A large volume of reserves and production allows the development of the ceramic sector. Kaolinite prices are influenced by the availability of reserves, geographic location (transport), and aggregate technology for processing and treatment (Pardo *et al.,* 2018; Illera *et al.,* 2015). Clay minerals are hydrated aluminum silicates made up of layers of SiO_2 tetrahedrons and Al_2O_3 octahedrons, which are intercalated in proportions: 1: 1 (kaolinite) and 2: 1 (montmorillonite) (Klunk *et al.,* 2019a). These minerals are part of the group defined as hydrated silicates, essentially made up of aluminum, in addition to iron, magnesium, and other impurities (Klunk *et al.,* 2019b).

Clay minerals are widely used in the industry. The use of these minerals as raw material results from the quality of the material produced. Kaolinites can present different degrees of purity and crystallinity due to cationic exchanges, with contaminants such as quartz and iron oxides (Klunk *et al.,* 2019c). Thus, the identification of the minerals present in the clays, as well as their physical-chemical characterization, are critical points in determining and understanding the behavior of the materials for the quality control of the final product (Ruosso *et al.,* 2019; Klunk *et al.,* 2019d; Klunk *et al.,* 2020a). Depending on the origin of the kaolinites, structural defects can occur due to the presence of iron oxides in its structure, being hematite (Fe_2O_3), and goethite (FeO(OH) - predominantly), the most common (Klunk *et al.,* 2020b). These compounds can be predicted through geochemical modeling using speciation of the elements (Klunk *et al.,* 2015; Klunk *et al.,* 2019e,f,g).

Thus, it is necessary to evaluate the potential of these materials for applications in the traditional ceramic industry. The goethite concentration is directly related to the depositional system. The availability of water promotes the concentration of humic acids, favoring the formation of FeO(OH) (Klunk *et al.,* 2012). Usually, Fe oxides have a high specific surface, resulting in high anion adsorption power, contributing to the kaolinite ion exchange capacity. However, few studies relate the influence of goethite with kaolinite, mainly on the effect on mineralogy (Fraga *et al.,* 2014).

Therefore, the objectives of this study are to relate the contents of goethite in kaolinite under different mixtures and to follow the evolution of the system through the techniques of XRF, XRD, Scanning Electron Microscopy (SEM) images allied to Spectrometer Energy Dispersive X-ray (EDS and RAMAN. The basic structural unit of iron oxides is associated with the octahedral arrangement, in which each iron atom is surrounded by six oxygen and hydroxyls, so the oxides are differentiated by the type of octahedral arrangement. In this way, it is possible to identify the occurrence of goethite in kaolinite by the manifestation of functional groups related to iron.

2. MATERIALS AND METHODS

2.1. Sistema de Mistura

The mixtures were performed with kaolinite:goethite, powered (mean diameter < 62 μm), with a weight proportion of 90:10 % with increments of 10 % in goethite until the proportion of 10:90 %, respectively.

2.2. Characterization of the Materials

2.2.1. X-Ray Fluorescence Spectroscopy

The chemical composition of the solid, liquid and gaseous materials can be easily determined by the X-Ray Fluorescence Spectroscopy (XRF), which allows the identification and quantification of chemical elements from almost the entire periodic table (Klunk *et al.,* 2015; Klunk *et al.,* 2018). When a sample is irradiated with primary X-Rays, the electron of the innermost layer of the atom is ejected, causing a void. The excited atom returns to the ground state through a series of electronic transitions. This electronic transition process emits characteristic fluorescent X-Rays. Such a phenomenon is known as X-Ray fluorescence (Elaiopoulos *et al.,* 2010).

Therefore, each element emits characteristic radiation (energy and wavelength defined) that are detected and used for qualitative analysis. The quantitative information of the elements present in the sample is directly related to the intensity of the radiation emitted (Elaiopoulos *et al.,* 2010).

The X-Ray fluorescence technique can be divided into dispersive wavelength (sequential or simultaneous), dispersive, and special energy categories (synchrotron radiation source, total reflection, and particle induction). The dispersive energy fluorescence (EDXRF) technique has a lower resolution than the wavelength dispersion technique (WDXRF), but it is also widely used for rapid and exploratory analysis (Somerset, 2004).

X-Ray Fluorescence by wavelength dispersion (WDXRF) using the fundamental parameters (FP) method provides semi-quantitative and multi-elemental analyzes, as well as being non-destructive and fast. This method relates the theoretical fluorescence intensity of the chemical elements by means of samples of known chemical composition and the measured fluorescent intensity, thus, being able to determine the unknown chemical composition (Caetano *et al.,* 2015a). The XRF technique is not very sensitive for the detection of light elements due to induced Auger emission that reduces the intensity of XRF in the sample (Caetano *et al.,* 2015b).

2.2.2. X-Ray Diffraction

The X-Ray Diffraction (XRD) technique has wide application in the field of material characterization due to the information it provides on the mineralogical composition, the arrangement of the atoms and the study of details of the lattice structures in crystalline of the various materials (Caetano *et al.,* 2015c; Cataluña *et al.,* 2018). To identification of the compounds present in kaolinite and Goethite, DRX is an indispensable tool because this type of material has several compounds in crystalline form. X-rays are generated both by the deceleration of the electrons in a metal target and by the excitation of the electrons of the target atoms. An electron bombarded copper target is considered a good target for producing a strong line to CuKα (Caetano *et al.,* 2018; Cataluña *et al.,* 2017).

The phenomenon of diffraction occurs because X-Rays are scattered around the ordered environment of a crystal, causing interference between X-Ray waves. Constructive and destructive interferences form patterns capable of providing information regarding the characteristics of the compounds present in a sample. Diffraction occurs when the wavelength of radiation is comparable to the characteristic spacings within the object that causes diffraction. Therefore, in order to obtain diffraction patterns of layers of atoms, it is necessary to use radiation having a wavelength comparable to the spacing of the layers, which is the case with X-Rays (Zhang *et al.,* 2018; Suzzoni *et al.,* 2018). The main diffraction methods are: i) Laue Method, which is used for the determination of crystal orientation in solid-state physics experiments; ii) Method of rotating crystal used for the determination of the configuration of enzymes, determination of the form of molecules, among other applications; and iii) Powder Method for Sprayed Samples (Pietzsch *et al.,* 2015; De Aza *et al.,* 2014).

In the diffraction technique by the powder method, a monochromatic X-Ray beam is directed to a sprayed sample, spread on a support, and the diffraction intensity is measured when a detector is moved at different angles. The pattern obtained is characteristic of the material in the sample and can be identified by comparison with standards base of data from ICDD (Joint Committee on Powder Diffraction Standards - JCPDS) da International Union of Crystallography (Cora *et al.,* 2014; Yan *et al.,* 2017).

Thus, XRD by the powder method provides a fingerprint of the sample. It can also be used to identify the size and type of the unit cell by measuring the spacing of the lines in the diffraction pattern (Miranda-Trevino and Coles, 2003).

The central equation for analyzing the results in a powder diffraction experiment is the Bragg equation ($2d \operatorname{sen} \theta = \lambda$); were, θ are the angles at which constructive interference occurs with the spacing d of the layers of atoms in the samples for X-rays of wavelength λ (Atkins e Jones, 2001). X-rays are reflected by the crystal only if the angle of incidence satisfies the condition established by Bragg's Law (Castrillo *et al.,* 2015; Zulfiqar *et al.,* 2015).

2.2.3. Scanning Electron Microscopy and Spectrometer Energy Dispersive X-ray

The morphology of materials can be studied by obtaining images through the Scanning Electron Microscopy (SEM) and Spectrometer Energy Dispersive X-ray (EDS) analysis, which provides micrographs at higher resolutions than

those provided by light microscopy, which is limited by diffraction effects of the order of magnitude of the wavelength of the light (Klunk *et al.,* 2019e; Rong *et al.,* 2008; Shahwan *et al.,* 2005; Frost *et al.,* 2002; Gupta *et al.,* 2011).

In a scanning electron microscope, the surface of a solid sample is swept with an electron beam. Samples that conduct electricity are easier to study because the free electron flow minimizes the charge accumulation and the possibility of thermal degradation of the sample. A number of techniques were developed to obtain electron microscopy images of non-conducting samples. The most common procedure involves coating the surface with a thin metallic film.

2.2.4. Raman Spectroscopy

Raman spectroscopy is a spectroscopic technique used to observe vibrational, rotational, and other low-frequency modes in a system (Frost *et al.,* 1997; Kloprogge, 2017). This technique is commonly used in chemistry to provide a structural fingerprint by which molecules can be identified (Khanna, 1981; Thibeau *et al.,* 1978; De Faria *et al.,* 2007; Clark and Curri, 1998; Oh *et al.,* 1998).

3. RESULTS AND DISCUSSION

3.1. Chemical Composition

The chemical composition of Kaolinite and Goethite with its respective mixtures was determined by XRF found in Figure 1. The present compounds are derived from the inorganic fraction in both Kaolinite and Goethite, and therefore, the results are presented in the form of oxides. According to Figure 1, there were large variations between the contents of the main components (kaolinite 100% and goethite 100%) of the different mixtures.

The content of the principal compounds forming the kaolinite structure are SiO_2 and Al_2O_3, and for goethite is Fe_2O_3 (in the form of oxide as read from the XRF equipment). For the kaolinite, the SiO_2 content varied from 52.80% (100% Kaolinite) to 6.58% (represented by the mixture of G90% + K10%) and the Al_2O_3 content ranged from 38.90% (100% Kaolinite) to 3.71 % (represented by the mixture of G90% + K10%).

Thus, for the compounds forming the goethite structure, the amount of Fe_2O_3 varied from 5.97% in the mixture of G 10% + K 90% to 84.42 in the mixture of G 90% + K 10%. Figure 1 shows all fractions of a mixture of kaolinite and goethite.

3.2. Mineralogical Composition

The technique of XRD allowed the identification of the crystalline phase's present kaolinite and goethite. Figure 2 shows the diffractograms of the samples of Kaolinite and Goethite (pattern and in the study), respectively.

The XRD pattern of the kaolinite sample is shown in Figure 2a. The spectrum of the kaolinite sample contains all the major peaks referring to (Joint Committee on Powder Diffraction Standards) JCPDS, database file (PDF-01-089-6538), thus indicating the formation of $Al_2Si_2O_5(OH)_4$. The main (hkl) indices of kaolinite like (001) and (002) are indicated in the pattern. The peaks are slightly broad, indicating a smaller crystal size (Phoebe and Medard 1991; Jehan *et al.,* 1970).

The XRD pattern of the goethite samples is shown in Figure 2b. The spectrum of the goethite sample contains all the major peaks referring to (Joint Committee on Powder Diffraction Standards) JCPDS, database file (PDF-17-0536), thus indicating the formation of α-FeOOH. The main (hkl) indices of goethite like (020), (110), (120), (130), (111), (121), (140) and (221) are indicated in the pattern. The peaks are slightly broad, indicating a smaller crystal size (Ghosh *et al.,* 2012).

The results of the XRD analysis indicate that in the samples of kaolinite (A) pattern and in the study, we showed the absence of goethite. Therefore, in the samples of goethite (B) pattern and in the study, we find the same behavior of absence of compounds of another nature, thus without traces of kaolinite.

The difference in relative intensity of the diffraction peaks found in the kaolinite and goethite pattern when compared to Kaolinite and Goethite in the study may indicate different proportions of the phases found, as may be the result of sample preparation in the X-ray diffraction tests. The discrepancies between the amounts of the compounds found in the different samples can be attributed to the different geological conditions in the formation of kaolinite and goethite in the study.

3.3. Morphology

The technique of Scanning Electron Microscopy (SEM) images allied to Spectrometer Energy Dispersive X-ray (EDS) analysis were used in this present work for the study of morphology. The objective is to complement the other characterization techniques in the evaluation of the shape of the particles and composition present in the samples. Figure 3 shows us the micrographics' of Kaolinite and Goethite in the study.

In Fig. 4 are the micrographies of the mixture of 50% kaolinite + 50% Goethite (A) with their respective EDS (B and C). At point 051 and 052 (Fig. 4A) the Spectrometer Energy Dispersive X-ray show particularity in the diffractogram. Characteristic of each mineral phase in the blend. Kaolinite is represented in EDS-051 and Goethite in EDS-052.

3.4. Raman Spectroscopy

The Raman spectroscopic analysis identified the phase of goethite (fig. 5). Raman bands occurring at 299, 400, 484, 550, and 674 cm^{-1} were assigned to the Fe-OH symmetric bend; Fe-O-Fe/-OH symmetric stretching; Fe-OH asymmetric stretching and Fe-O symmetric stretching, respectively (Dunnwald and Otto 1989; Kieser et al., 1983; Boucherit et al., 1991). As the amount of kaolinite increases in the mixture, the RAMAN spectrum reveals a decrease in Goethite band.

4. CONCLUSIONS

With the results obtained from techniques used allowed the following conclusions to be drawn:

- XRD identified crystalline phases of Kaolinite and Goethite;

- XRF showed the compounds present and derived from the mixture fraction in both Kaolinite and Goethite;

- SEM-EDS showed the grain morphology in the Kaolinite mixture 50% + Goethite 50% with the respective compositions);

- RAMAN (reveals a decrease of Goethite peaks as the percentage of Kaolinite increases in the mixture) made it possible to characterize Kaolinite and Goethite in a mixing system.

We show in this research the potential of spectroscopy in the identification and quantification of mineral kaolinite in mixtures with mineral Fe. We conclude that kaolinite can be identified and quantified with a high correlation in the mix from the depth of the main diagnostic absorption feature with little sample preparation. Thus, the method has great potential to assist in quantification and, consequently, in the discrimination of kaolinite quality.

With little or no sample preparation, the spectroscopy can be used in obtaining many important information of mineralogy. The spectroscopy is a non-expensive, fast, and non-evasive, or little evasive methodology that offers great potential for the identification and qualification of minerals and mix.

5. ACKNOWLEDGMENTS

This project was financially supported by the projects Modelagem Digital de Afloramentos utilizando GPU (MCT/FINEP - Pré-Sal Cooperativos ICT - Empresas 03/2010 - Contract 01.23.4567.89) and FINEP-PROINFRA (Contract: 01.13.0302.00). MKS thanks PROSUP/CAPES for the financial support of the Ph.D. scholarship. MRV thanks the Brazilian Council for Scientific and Technological Development (CNPq) for the research grant (Process 309399/2014-9).

6. REFERENCES

1. Schrecker, T., Birn, A.-E., Aguilera, M. How extractive industries affect health: Political economy underpinnings and pathways. *Health & Place*, **2018**, 52, 135–147.
2. Giacomin, A. M., Garcia, J. B., Zonatti, W. F., Silva-Santos, M. C., Laktim, M. C., Baruque-Ramos, J. Brazilian silk production: economic and sustainability aspects. *Procedia Engineering,* **2017**, 200, 89–95.
3. Paulino, E. T. The agricultural, environmental and socio-political repercussions of Brazil's land governance system. *Land Use Policy,* **2014**, 36, 134–144.
4. Macedo, A. B., de Almeida Mello Freire, D. J., Akimoto, H. Environmental management in the Brazilian non-metallic small-scale mining sector. *Journal of*

Cleaner Production, **2003**,11(2), 197–206.
5. De Souza, C. A. R., Souza, A. M., Souza, F. M., da Veiga, C. P., da Silva, W. V. The importance of principal components in studying mineral prices using vector autoregressive models: Evidence from the Brazilian economy. *Resources Policy,* **2019**, 62, 9–21.
6. Sruthi, P. L., Reddy P, H. P. Characterization of kaolinitic clays subjected to alkali contamination. *Applied Clay Science,* **2017**, 146, 535–547.
7. Pardo, F., Jordan, M. M., Montero, M. A. Ceramic behaviour of clays in Central Chile. *Applied Clay Science,* **2018**, 157, 158–164.
8. Illera, L. C., Illera, C. C., Contreras, K. A. Raw material for the ceramic industry in Norte de Santander. III. Assessment of the technological properties when the residue test of deep abrasion is added. *Boletín de La Sociedad Española de Cerámica y Vidrio,* **2015**, 54(2), 77–83.
9. Klunk, M.A., Shah, Z., Wander, P.R. Use of Montmorillonite Clay for Adsorption Malachite Green Dye. *Periódico Tchê Química,* **2019a**, 16(32), 279-286.
10. Klunk, M.A., Dasgupta, S., Nunes, B.V.G., Wander, P.R. Synthesis of Sodalite Zeolite to Treatment of Textile Effluents. *Periódico Tchê Química,* **2019b**, 16(31), 778-783.
11. Klunk, M. A., Dasgupta, S., Das, M., Wander, P. R., Shah, Z., Adsorption Study of Crystal Violet and Malachite Green Dyes in Zeolitic Material. *Periódico Tchê Química,* **2019c**, 16(33), 70-81.
12. Ruoso, F. S., Bittencourt, L. C., Sudati, L. U., Klunk, M. A., Caetano, N. R. New Parameters for the Forest Biomass Waste Ecofirewood Manufacturing Process Optimization. Periódico Tchê Química, **2019**, 16(32), 560-571.
13. Klunk, M. A., Dasgupta, S., Das, M., Cunha, M. G., Wander, P. R. Synthesis of Sodalite Zeolite and Adsorption Study of Crystal Violet Dye. *ECS Journal of Solid State Science and Technology,* **2019d**, 8(10), N144–N150.
14. Klunk, M. A., Das, M., Dasgupta, S., Impiombato, A. N., Caetano, N. C., Wander, P. R., Moraes, C. A. M. Comparative study using different external sources of aluminum on the zeolites synthesis from rice husk ash. Materials Research Express, **2020a**, 7, 015023.
15. Klunk, M. A., Schröpfer, S. B., Dasgupta, S., Das, M., Caetano, N. R., Impiombato, A. N., Wander, P. R., Moraes, C. A. M. (2020B). Synthesis and characterization of mordenite zeolite from metakaolin and rice husk ash as a source of aluminium and silicon. *Chemical Papers,* **2020b**, 74, 2481-2489.
16. Klunk, M. A., Damiani, L. H., Feller, G., Rey, M. F., Conceiçao, R. V., Abel, M., De Ros, L. F. Geochemical modeling of diagenetic reactions in Snorre Field reservoir sandstones: a comparative study of computer codes. Brazilian Journal of Geology, **2015**, 45, 29-40.
17. Klunk, M. A., Dasgupta, S., Schropfer, S. B., Nunes, B. V. G., Wander, P. R. Comparative Study of Geochemical Speciation Modeling Using GEODELING Software. Periódico Tchê Química, **2019e**, 16(31), 816-822.
18. Klunk, M. A., Dasgupta, S., Das, M., Wander, P. R. Computer Codes of Geochemical Modeling used to Water-Rock Interaction Simple and Complex Systems. Periódico Tchê Química, **2019f**, 16(32), 108-118.
19. Klunk, M. A., Dasgupta, S., Das, M., Wander, P. R., Di Capua, A. Geochemical Speciation and Batch Mode Simulation in the Carbonate Depositional Environments. Periódico Tchê Química, **2019g**, 16(33), 736-748.
20. Klunk, M. A., Oliveira, A., Furtado, G., Knornschild, G. H., Dick, L. F. P. Study of the Corrosion of Buried Steel Grids of Electrical Power Transmission Towers. *ECS Transactions,* **2012**, 43, 23-27.
21. Fraga, A., Klunk, M. A., Oliveira, A., Furtado, G., Knornschild, G. H., Dick, L.F.P. Soil corrosion of the AISI1020 steel buried near electrical power transmission line towers. *Materials Research,* **2014**, 17, 1637-1643, 2014.
22. Klunk, M. A., Damiani, L. H., Feller, G., Rey, M. F., Conceiçao, R. V., Abel, M., De Ros, L. F. Geochemical modeling of diagenetic reactions in Snorre Field reservoir sandstones: a comparative study of computer codes. *Brazilian Journal of Geology,* **2015**, 45, 29-40.
23. Klunk, M. A., Dasgupta, S., Conceiçao, R. V. Computerized geochemical modeling of burial diagenesis of the Eocene turbidite reservoir elements: Urucutuca Formation, Espírito Santo Basin, southeastern Brazil passive margin. Journal of Palaeogeography, **2018**, 7, 12-26.
24. Elaiopoulos, K., Perraki, T., Grigoropoulou,

E. Monitoring the effect of hydrothermal treatments on the structure of a natural zeolite through a combined XRD, FTIR, XRF, SEM and N2-porosimetry analysis. *Microporous and Mesoporous Materials*, **2010**, 134(1-3), 29–43.
25. Somerset, V. The use of X-ray fluorescence (XRF) analysis in predicting the alkaline hydrothermal conversion of fly ash precipitates into zeolites. Talanta, **2004**, 64(1), 109–114.
26. Caetano, N. R., Cataluña, R., Vielmo, H. A. Analysis of the Effect on the Mechanical Injection Engine Using Doped Diesel Fuel by Ethanol and Bio-Oil. *International Review of Mechanical Engineering,* **2015a**, 9(2), 124–128.
27. Caetano, N. R., Soares, D., Nunes, R. P., Pereira, F. M., Schneider, P. S., Vielmo, H. A., van der Laan, F. T. A comparison of experimental results of soot production in laminar premixed flames. *Open Engineering,* **2015b**, 5, 213–219.
28. Caetano, N. R., Stapasolla, T. Z., Peng, F. B., Schneider, P. S., Pereira, F. M., Vielmo, H. A. Diffusion Flame Stability of Low Calorific Fuels. *Defect Diffusion Forum*, **2015c**, 362, 29–37.
29. Cataluña, R., Shah, Z., Venturi, V., Caetano, N. R., Da Silva, B. P., Azevedo C. M. N., Da Silva, R., Suarez, P. A. Z., Oliveira, L. P. Production process of di-amyl ether and its use as an additive in the formulation of aviation fuels. *Fuel*, **2018**, 228, 226–233.
30. Caetano, N. R., Venturini, M. S., Centeno, F. R., Lemmertz, C. K., Kyprianidis, K. G. Assessment of mathematical models for prediction of thermal radiation heat loss from laminar and turbulent jet non-premixed flames. *Thermal Science and Engineering Progress,* **2018**, 7, 241–247.
31. Cataluña, R., Shah, Z., Pelisson, L., Caetano, N. R., Da Silva, R., Azevedo, C. Biodiesel Glycerides from the Soybean Ethylic Route Incomplete Conversion on the Diesel Engines Combustion Process. *Journal of the Brazilian Chemical Society*, **2017**, 28(12), 2447–2454.
32. Zhang, Q., Yan, Z., Ouyang, J., Zhang, Y., Yang, H., Chen, D. Chemically modified kaolinite nanolayers for the removal of organic pollutants. *Applied Clay Science*, **2018**, 157, 283–290.
33. Suzzoni, A., Barre, L., Kohler, E., Levitz, P., Michot, L. J., M'Hamdi, J.. Interactions between kaolinite clay and AOT. *Colloids and Surfaces A: Physicochemical and Engineering Aspects*, **2018**, 556, 309–315.
34. Pietzsch, A., Nisar, J., Jämstorp, E., Gråsjö, J., Århammar, C., Ahuja, R., Rubensson, J.-E. Kaolinite: Defect defined material properties – A soft X-ray and first principles study of the band gap. *Journal of Electron Spectroscopy and Related Phenomena,* **2015**, 202, 11–15.
35. De Aza, A. H., Turrillas, X., Rodriguez, M. A., Duran, T., Pena, P. Time-resolved powder neutron diffraction study of the phase transformation sequence of kaolinite to mullite. *Journal of the European Ceramic Society*, **2014**, 34(5), 1409–1421.
36. Cora, I., Dódony, I., Pekker, P. Electron crystallographic study of a kaolinite single crystal. *Applied Clay Science*, **2014**, 90, 6–10.
37. Yan, K., Guo, Y., Fang, L., Cui, L., Cheng, F., Li, T. Decomposition and phase transformation mechanism of kaolinite calcined with sodium carbonate. *Applied Clay Science,* **2017**, 147, 90–96.
38. Miranda-Trevino, J. C., Coles, C. A. Kaolinite properties, structure and influence of metal retention on pH. *Applied Clay Science,* **2003**, 23(1-4), 133–139.
39. Franco, F. The influence of ultrasound on the thermal behaviour of a well ordered kaolinite. *Thermochimica Acta*, **2003**, 404(1-2), 71–79.
40. Atkins, P.; Jones, L. Princípios de Química – questionando a vida moderna e o meio ambiente. Porto Alegre: Bookman, **2001**.
41. Castrillo, P. D., Olmos, D., & González-Benito, J. Kinetic study of the intercalation process of dimethylsulfoxide in kaolinite. International *Journal of Mineral Processing,* **2015**, 144, 70–74.
42. Zulfiqar, S., Sarwar, M. I., Rasheed, N., & Yavuz, C. T. Influence of interlayer functionalization of kaolinite on property profile of copolymer nanocomposites. *Applied Clay Science,* **2015**, 112-113, 25–31.
43. Klunk, M. A., Shah, Z., Caetano, N. R., Conceição, R. V., Wander, P. R., Dasgupta, S., Das, M. CO_2 sequestration by magnesite mineralization through interaction between Mg-brine and CO_2 : integrated laboratory experiments and computerized geochemical modelling. *International Journal of Environmental Studies*, **2019e**, 1-18.
44. Rong, X., Huang, Q., He, X., Chen, H., Cai,

P., Liang, W. Interaction of Pseudomonas putida with kaolinite and montmorillonite: A combination study by equilibrium adsorption, ITC, SEM and FTIR. *Colloids and Surfaces B: Biointerfaces,* **2008**, 64(1), 49–55.
45. Shahwan, T., Zünbül, B., Tunusoğlu, Ö., Eroğlu, A. E. AAS, XRPD, SEM/EDS, and FTIR characterization of Zn2+ retention by calcite, calcite–kaolinite, and calcite–clinoptilolite minerals. *Journal of Colloid and Interface Science*, **2005,** 286(2), 471–478.
46. Frost, R. L., Van Der Gaast, S. J., Zbik, M., Kloprogge, J. T., Paroz, G. N. Birdwood kaolinite: a highly ordered kaolinite that is difficult to intercalate—an XRD, SEM and Raman spectroscopic study. *Applied Clay Science*, **2002**, 20(4-5), 177–187.
47. Gupta, V., Hampton, M. A., Stokes, J. R., Nguyen, A. V., Miller, J. D. Particle interactions in kaolinite suspensions and corresponding aggregate structures. *Journal of Colloid and Interface Science*, **2011**, 359(1), 95–103.
48. Frost, R. L., Thu Ha, T., & Kristof, J. FT-Raman spectroscopy of the lattice region of kaolinite and its intercalates. *Vibrational Spectroscopy*, **1997**, 13(2), 175–186.
49. Kloprogge, J. T. Raman and Infrared Spectroscopies of Intercalated Kaolinite Groups Minerals. *Infrared and Raman Spectroscopies of Clay Minerals*, **2017**, 343–410.
50. Khanna, R. K. Raman-spectroscopy of oligomeric SiO_2 species isolated in solid methane. *Journal of Chemical Physics*, **1981**, 74 (4), 2108.
51. Thibeau, R. J., Brown, C. W., Heidersbach, R. H. Raman spectra of possible corrosion products of iron. *Applied Spectroscopy*, **1978**, 32, 532–535.
52. De Faria, D. L. A., Lopes, F. N. Heated goethite and natural hematite: Can Raman spectroscopy be used to differentiate them? *Vibrational Spectroscopy*, **2007**, 45(2), 117–121.
53. Clark, R. J. H., Curri, M. L. The identification by Raman microscopy and X-ray diffraction of iron-oxide pigments and of the red pigments found on Italian pottery fragments. *Journal of Molecular Structure*,**1998**, 440, 105–111.
54. Oh, S. J., Cook, D. C., Townsend, H. E. Characterization of iron oxides commonly formed as corrosion products on steel. *Hyperfine Interactions*,**1998**, 112, 59–65.
55. Phoebe, H., Medard, T. A method combining SWIR and XRD for the identification of clay minerals; I, Interstratified kaolinite/smectite clays: Program and Abstracts - 28th Annual Clay Minerals Conference, Clay Minerals Society, **1991**, 28, 69.
56. Jehan, K., Qaiser, M. A., Khan, A. H. Quantitative estimation of kaolinite in clays by differential thermal analysis. *Pakistan Journal of Scientific and Industrial Research*, **1970**, 13(1-2), 169-173.
57. Ghosh, M. K., Poinern, G. E. J., Issa, T. B., Singh, P. Arsenic adsorption on goethite nanoparticles produced through hydrazine sulfate assisted synthesis method. Korean *Journal of Chemical Engineering*, **2012**, 29(1), 95-102.
58. Dunnwald, J., Otto, A. An investigation of phase transitions in rust layers using raman spectroscopy. *Corrosion Science*, **1989**, 29(9), 1167-1176.
59. Kieser, J. T., Brown, C. W., Heidersbach, R. H. Characterization of the passive film formed on weathering steels. *Corrosion Science*, **1983**, 23(3), 251-259.
60. Boucherit, N., Hugot-Le, Goff, A., Joiret, S. Raman studies of corrosion films grown on Fe and Fe-6Mo in pitting conditions. *Corrosion Science*, **1991**, 32(5-6), 497-507.

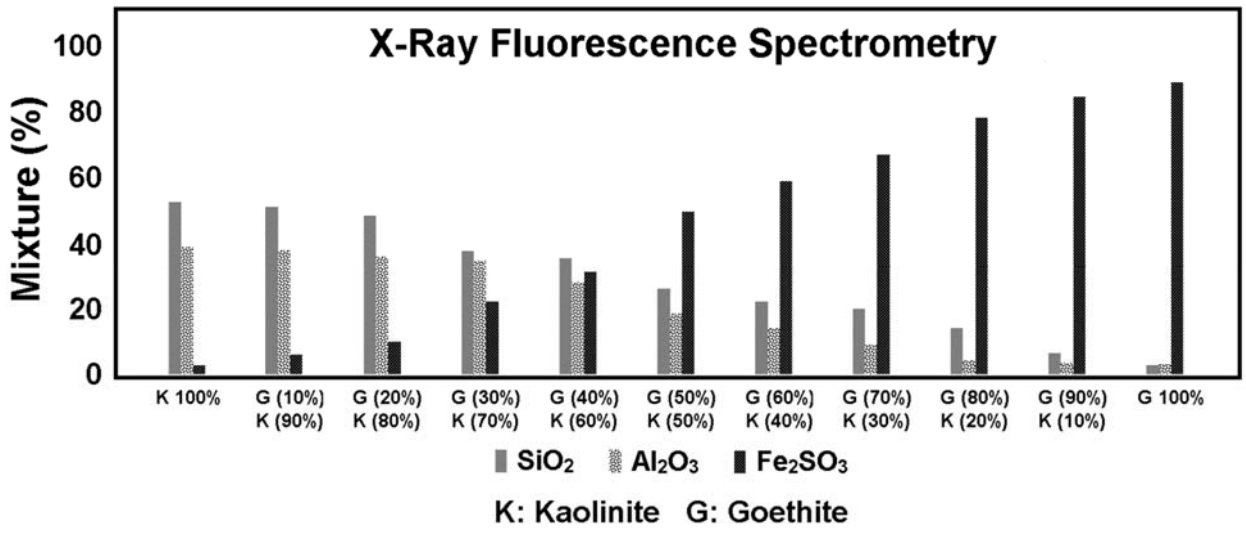

Figure 1. *XRF of kaolinite (K) and goethite (G) with mixture respective.*

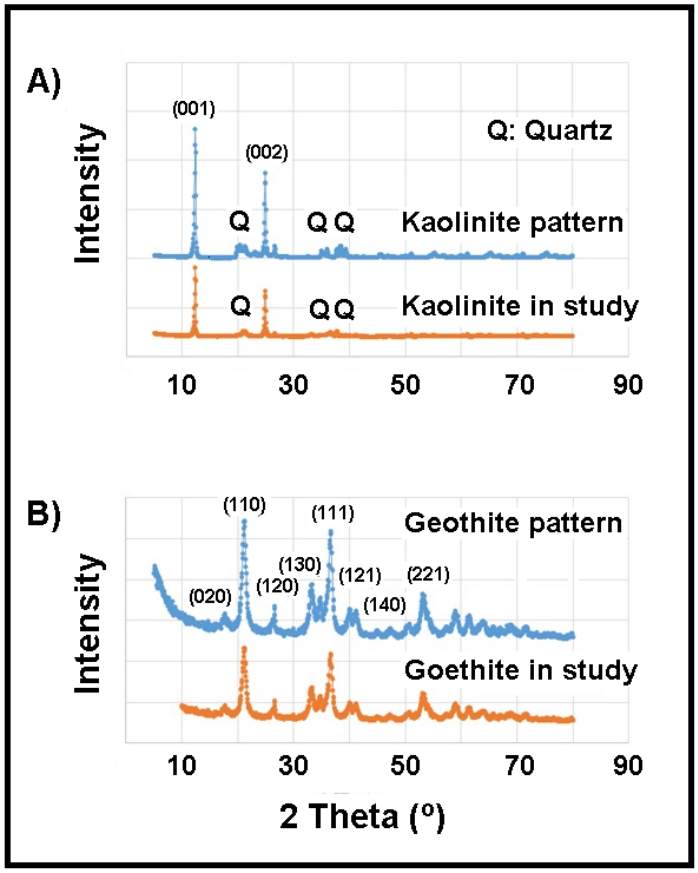

Figure 2. *XRD of kaolinite (a) and goethite (b).*

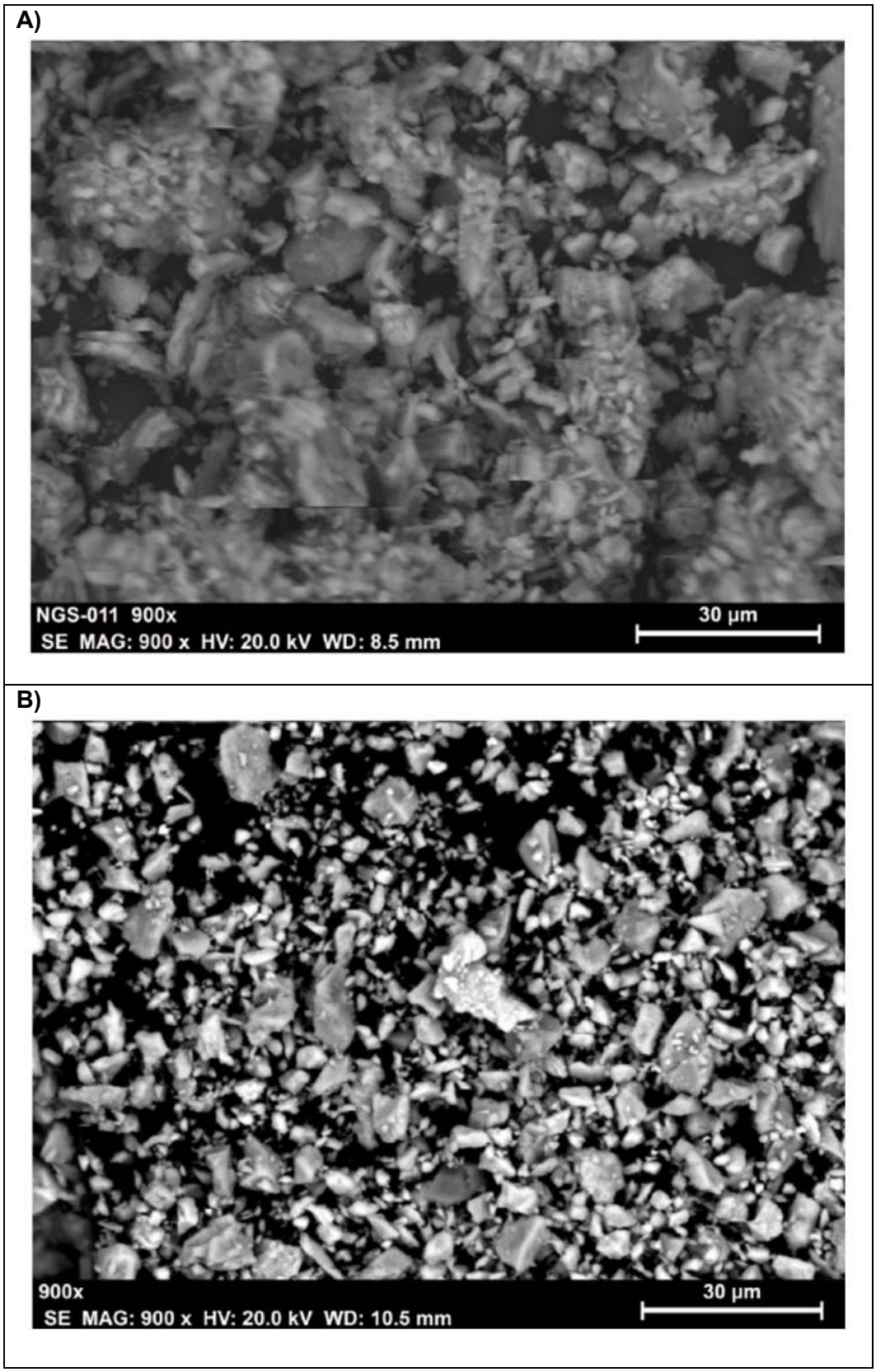

Figure 3. *SEM* of kaolinite *in study* (**A**), goethite in study (**B**).

A)

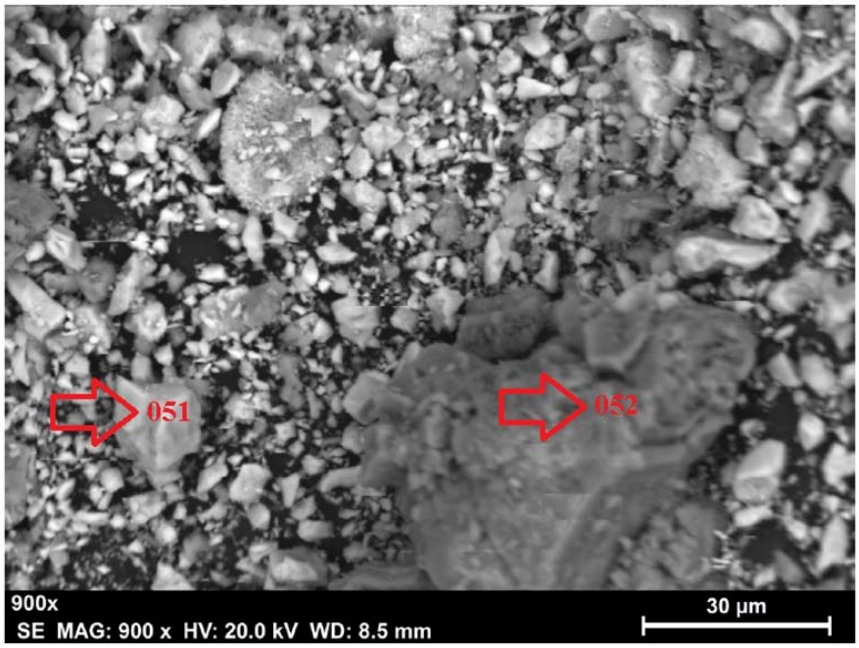

B)

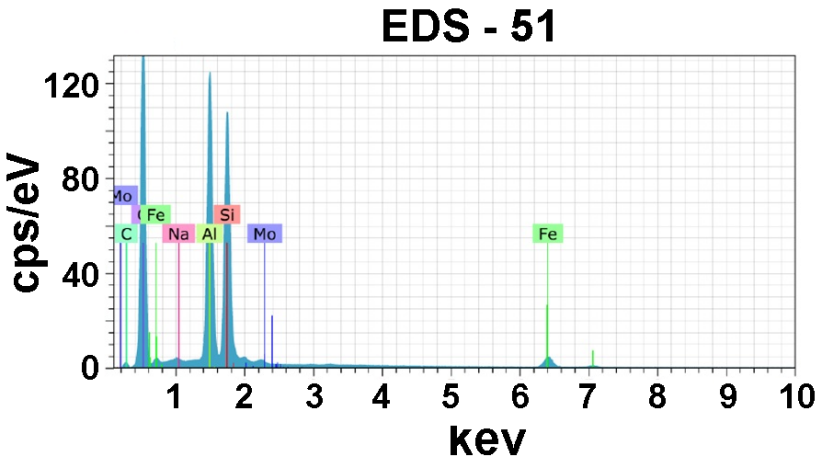

C)

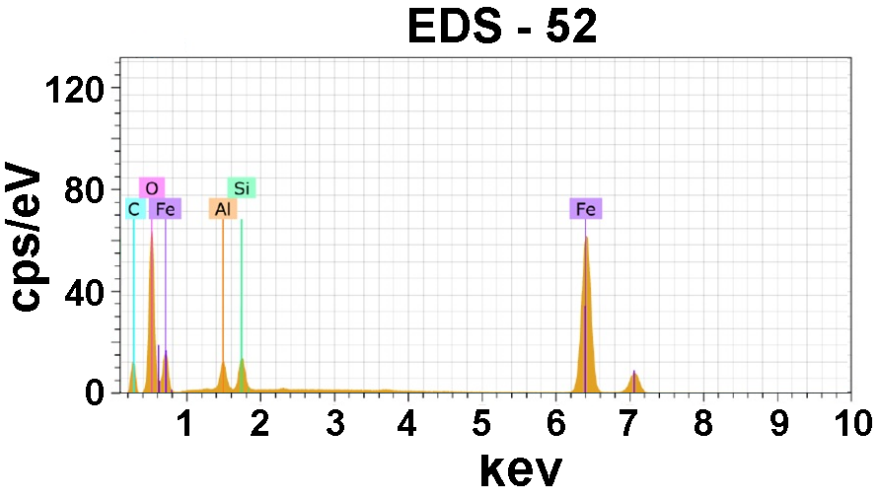

Figure 4. *SEM of the mixture 50% kaolinite + 50% goethite (A) in study with yours EDS (B and C).*

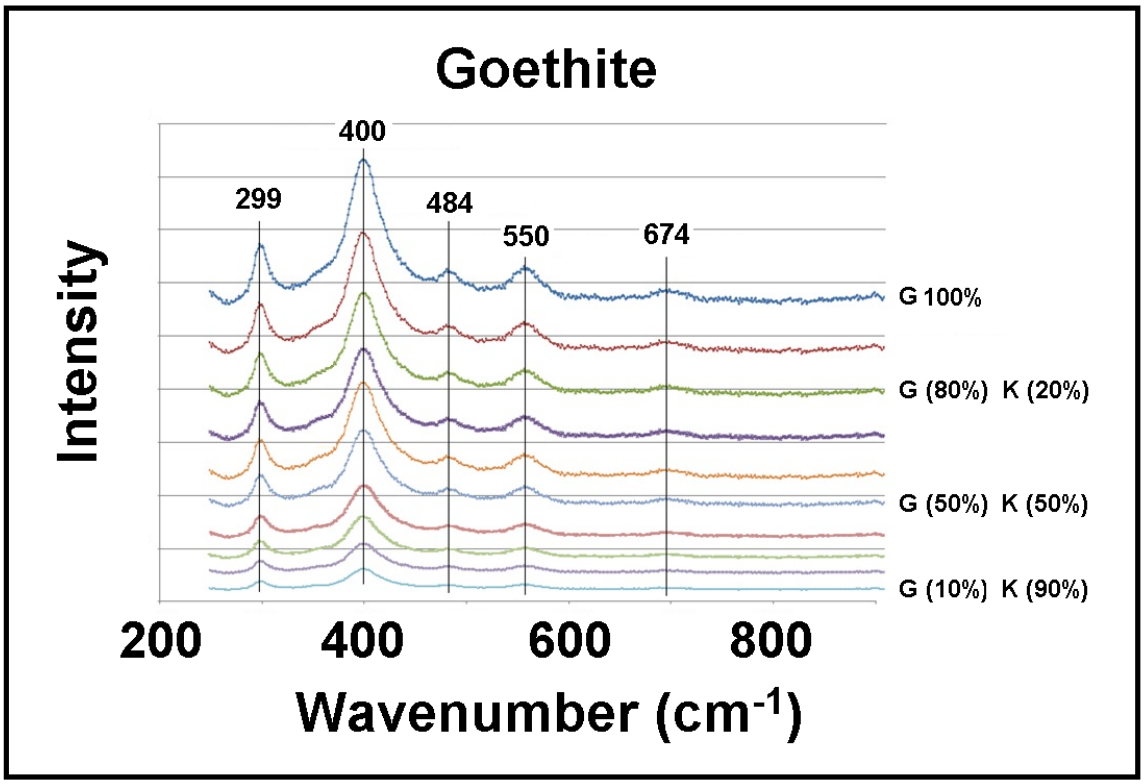

Figure 5. *Raman spectroscopic of goethite in the study (100%) plus a mixture of the kaolinite.*